



Copper (II) complexes with novel Schiff-based ligands: synthesis, crystal structure, thermal (TGA–DSC/FT-IR), spectroscopic (FT-IR, UV-Vis) and theoretical studies

Jeniffer Meyer Moreira¹ · Guilherme Fava Campos¹ · Leandro Moreira de Campos Pinto² · Gabriel Rodrigues Martins² · Bárbara Tirloni³ · Cristiane Storck Schwalm¹ · Cláudio Teodoro de Carvalho¹

Received: 29 January 2021 / Accepted: 29 March 2021
© Akadémiai Kiadó, Budapest, Hungary 2021

Abstract

This study aimed to synthesize two novel Schiff-base ligands through the condensation between *N*-(2-aminoethyl)pyrazoles and 2-hydroxy-1-naphthaldehyde, which are: NaphPz ((E)-1-(((2-(1H-pyrazol-1-yl)ethyl)imino)methyl)naphthalen-2-ol)) and NaphDPz ((E)-1-(((2-(3,5-dimethyl-1H-pyrazol-1-yl)ethyl)imino)methyl)naphthalen-2-ol). These novel pyrazole-imines were synthesized, characterized and used as copper (II) ion complexing agents. Different synthetic routes have been adapted to obtain the [Cu(NaphPz)Cl], [Cu(NaphDPz)Cl] and [Cu(NaphPz)₂] complexes in the solid state, the first two in the crystalline form and the latter as a powder. The minimum metal–ligand stoichiometry for the three complexes was defined by TGA–DSC thermoanalytical data and by single-crystal X-ray diffraction for the crystalline samples which belong to the *P*2₁/*n* space group. The products of the thermal decomposition of the material were also monitored by TGA–DSC/FT-IR in air and N₂ atmospheres in order to suggest how thermal decomposition of the organic portion of the complex occurs. Density functional theory (DFT) and time-dependent density functional theory (TD-DFT) calculations compared to experimental results (UV-Vis and FT-IR) show a high degree of correlation. From HOMO/LUMO orbitals, the main major charge distributions, responsible for the absorption bands of the complexes, were determined.

Keywords Synthesis · Schiff bases · TGA–DSC/FT-IR · Crystal structure · Theoretical calculation

Introduction

Pyrazole derivatives have a wide range of important biological activities, which give them a large number of pharmaceutical applications [1–3]. Due to such functionalities, the synthesis and characterization of pyrazole derivatives is an area of research that has attracted much attention from scientific community [4]. Concomitantly, pyrazole-imine derivatives have also been used as complexing agents and the combination of the imine moiety with other coordinating

groups leads to mono-, di-, tri- or multidentate ligands, which can be strategically designed to stabilize different metal centers with varying oxidation numbers [5]. Imines with RR'C=NR'' structure, where R'' can be an H substituent or an organic group are known as Schiff's bases, and these molecules containing a C=N bond, derived from the condensation between primary amines with a ketone or aldehyde, give rise to a family of compounds known to present interesting biological activities and a very extensive coordination chemistry; in some cases, the complexation of these molecules to a metallic center enhances the intrinsic biological effects of these compounds [6]. In the area of coordination chemistry, Schiff bases are considered quite versatile ligands, since their synthesis is simple and modular, allowing to modify the steric and electronic properties around the coordination site with some ease, just varying the aldehyde or ketone used in the condensation reaction.

In this context, the synthesis of polydentate pyrazole-imine hybrid derivatives presents itself as an interesting and promising proposal, since it can lead to compounds with

✉ Cláudio Teodoro de Carvalho
claudiocarvalho@ufgd.edu.br

¹ Federal University of Grande Dourados, UFGD, CP 364, Dourados, MS 79804–970, Brazil

² Federal University of Mato Grosso do Sul, Campo Grande, MS 79074-460, Brazil

³ Federal University of Santa Maria, UFSM, Santa Maria, RS 97105-900, Brazil

potential biological activities and applications in catalysis. Silva et al. [7] reported the synthesis of three pyrazole-imines derived from salicylaldehydes, in which the pyrazole ring is joined to the imine function by a bis-methylene bridge. The ligands were used to complex the gallium(III) ions in the presence of triethylamine and NH_4PF_6 , using methanol as a solvent. In this work, three gallium complexes with a general formula equal to $[\text{GaL}_2]\text{PF}_6$, where pyrazole-imine (L) acts as a monoanionic tridentate ligand, were obtained and evaluated for cytotoxicity against human carcinoma cells. Fe^{II} , Co^{II} , Ni^{II} , Zn^{II} and Cr^{III} complexes with pyrazole-imine ligands containing three coordination sites have also been obtained and successfully used as catalysts in ethylene oligomerization and polymerization reactions [8, 9]. Finally, Gama et al. [10] reported a study involving pyrazole-imine complexes with copper(II) ions, obtained by equimolar reactions of tridentate pyrazole-imines and $\text{CuCl}_2 \cdot \text{H}_2\text{O}$. All isolated complexes presented a minimum formula equal to CuLCl , where L represents a pyrazol-imine ligand. Analyzes by single-crystal X-ray diffraction allowed to observe that, in the solid state, the complexes derived from a dichlorinated pyrazole-imine and its analog diiodinated have distinct crystalline structures. According to the data obtained, one complex has a dinuclear structure with distorted pyramidal quadratic geometry, while the other has a quadratic geometry.

As reported, pyrazole-imine compounds and their derivatives can be versatile candidates with potential for several applications, ranging from biological activities to use in important industrial processes, such as oligomerization and polymerization. Therefore, considering this perspective, this study had as its primary objective the synthesis and characterization of two novel Schiff-base ligands and their complexation with copper (II) ions for development of further studies related to their applications.

The three coordination complexes obtained: $[\text{Cu}(\text{NaphPz})]$, $[\text{Cu}(\text{NaphPz})\text{Cl}]$ and $[\text{Cu}(\text{NaphDPz})\text{Cl}]$, were characterized using thermoanalytical data from TGA–DSC/DTG, TGA/FT-IR and single-crystal X-ray diffraction data for the chlorinated complexes obtained as a single crystal. Theoretical calculations were also performed for all complexes using time-dependent density-functional theory (TDDFT), supported by experimental data from UV-Vis and FT-IR and, show consequently how charge transfers occur in systems through HOMO/LUMO molecular orbitals.

Experimental

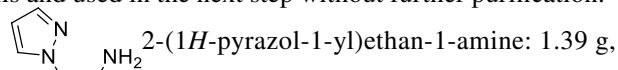
Synthesis of the ligands (adapted from Hamann and Tuzcek [11])

Preparation of free 2-chloroethanamine solution from the corresponding hydrochloride

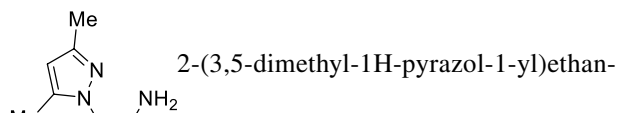
A suspension containing 2.784 g of 2-chloroethanamine hydrochloride (24 mmol) in 8 mL of acetonitrile was prepared in a 25-mL round bottom flask, which was cooled to 0°C (controlled by thermometer) using an ice bath. At this temperature, 3.35 mL of triethylamine (24 mmol) were dropwise added to the suspension under magnetic stirring and, after the end of the addition, the reaction mixture was kept under stirring at this low temperature for 1 h. The crude reaction mixture was then filtered, employing minimal amounts of acetonitrile for washing of the inorganic residue, and the filtrate containing the desired free 2-chloroethanamine was reserved for direct use in the next reaction step without further manipulation.

N-alkylation of pyrazoles

To a 50-mL round bottom flask were added 16 mmol of the corresponding pyrazole (1.09 g of 1*H*-pyrazole or 1.538 g of 3,5-dimethyl-1*H*-pyrazole), 8 mL of acetonitrile and 1.92 g of NaOH (48 mmol), and the resulting suspension was kept under magnetic stirring at room temperature for 30 min. After this period, the temperature was raised to 75°C using an oil bath and the filtrate from the previous step was added dropwise into the reaction vessel; after the end of the addition, the reaction mixture was kept under heating and stirring for 5 h, then cooled down to room temperature, filtered and the filtrate was concentrated under reduced pressure (rotatory evaporator) to remove the solvent and excess volatile reagents. Through this procedure, the *N*-alkylated pyrazoles were obtained as yellowish viscous oils and used in the next step without further purification.

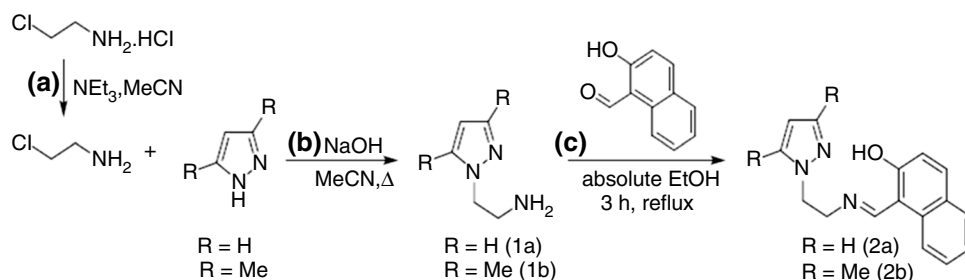


78% yield. $^1\text{H NMR}$: δ 7.50 (*d*, $J = 1.5$ Hz, 1H); 7.41 (*d*, $J = 2.1$ Hz, 1H); 6.23 (*t*, $J = 2.1$ Hz, 1H); 4.20–4.11 (*m*, 2H); 3.18–3.07 (*m*, 2H). $^{13}\text{C NMR}$: δ 139.7; 129.7; 105.5; 55.1; 42.3. FT-IR: 3364, 3297 (ν N–H).



2.2 g, quantitative yield. $^1\text{H NMR}$: δ 5.73 (*s*, 1H); 3.94 (*t*, $J = 6.0$ Hz, 2H); 3.02 (*t*, $J = 6.0$ Hz, 2H); 2.17

Fig. 1 Schematic diagram for the synthesis of ligands NaphHPz and NaphHDPz

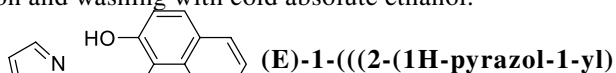


(*s*, 3H); 2.14 (*s*, 3H). $^{13}\text{C NMR}$: δ 147.5; 139.1; 105.0; 51.2; 42.1; 13.4; 11.1. **FT-IR**: 3361, 3297 (ν N–H).

48.6; 13.7; 11.0. **FT-IR**: 1616, 1544, 1355, 1206, 760. Melting point: 124 °C (Fig. 1).

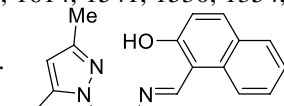
Schiff base formation (condensation with 2-hydroxy-1-naphthaldehyde)

To a 10-mL round bottom flask were added 3 mmol of the appropriate *N*-alkylated pyrazole, 542.4 mg of 2-hydroxy-1-naphthaldehyde (3.15 mmol) and 3 mL of absolute ethanol. The resulting reaction mixture was then subjected to magnetic stirring, under reflux conditions for 3 h. After this period, the crude reaction mixture was cooled down, either at room temperature or at approximately 20 °C to furnish the desired products as solids after vacuum filtration and washing with cold absolute ethanol.



(E)-1-(((2-(1H-pyrazol-1-yl)ethyl)imino)methyl)naphthalen-2-ol (NaphHPz): precipitated as a microcrystalline yellow solid after 2 h at room temperature; 560 mg, 70% yield. $^1\text{H NMR}$: δ 14.56 (*s*, 1H); 8.46 (*s*, 1H); 7.82–7.67 (*m*, 2H); 7.67–7.55 (*m*, 2H); 7.47–7.39 (*m*, 1H); 7.36 (*d*, $J = 2.1$ Hz, 1H); 7.32–7.19 (*m*, 1H); 6.98 (*d*, $J = 9.2$ Hz, 1H); 6.16 (*t*, $J = 2.1$ Hz, 1H); 4.46 (*t*, $J = 5.4$ Hz, 2H); 4.10 (*t*, $J = 5.4$ Hz, 2H). $^{13}\text{C NMR}$: δ 172.1; 160.7; 140.6; 136.6; 133.4; 130.8; 129.3; 128.0; 126.8; 123.2; 123.1; 118.5; 107.6; 105.9; 54.7; 52.6. **FT-IR**: 1626, 1614, 1541, 1530, 1354,

1180, 754. Melting point: 140 °C.



(E)-1-(((2-(3,5-dimethyl-1H-pyrazol-1-yl)ethyl)imino)methyl)naphthalen-2-ol (NaphHDPz): precipitated as an amorphous brownish solid after overnight refrigeration of the crude reaction at approximately 20 °C (freezer); 700 mg, 80% yield. $^1\text{H NMR}$: δ 8.26 (*s*, 1H); 7.64 (*d*, $J = 8.4$ Hz, 1H); 7.61 (*dd*, $J = 8.0, 1.1$ Hz, 1H); 7.40 (*ddd*, $J = 8.4, 7.0, 1.4$ Hz, 1H); 7.24 (*ddd*, $J = 7.9, 7.1, 1.0$ Hz, 1H); 6.93 (*d*, $J = 9.3$ Hz, 1H); 5.66 (*s*, 1H); 4.30–4.21 (*m*, 2H); 4.08–4.00 (*m*, 2H); 2.26 (*s*, 3H); 2.09 (*s*, 3H). $^{13}\text{C NMR}$: δ 174.0; 160.3; 148.7; 140.8; 137.1; 133.6; 129.3; 128.0; 126.6; 123.9; 123.1; 118.3; 107.3; 105.5; 53.7;

Synthesis of the complexes

Synthesis of the $[(\text{Cu}(\text{NaphPz})_2)]$ complex

In this synthetic route, firstly it was obtained the copper (II) carbonate, prepared by electrolysis process using a 12 V 2A switching power supply and two copper electrodes (copper wire). The electrodes were immersed in 50 mL of 5% sodium hydrogen carbonate suspension for two hours until complete formation of blue precipitate or the reaction stops. The precipitate obtained was washed with distilled water on Whatman n° 40 filter paper, until elimination of sodium ions and drying. In complexation reaction, 91 mg of (E)-1-(((2-(1H-pyrazol-1-yl)ethyl)imino)methyl)naphthalen-2-ol ligand (NaphHPz), in excess, were solubilized in a small portion of ethanol and added to a 25 mL reaction flask containing 8 mL of a 1: 1 mixture (ethanol and water) and 23 mg of CuCO_3 . The flask was then adapted to a reflux condenser and heated in oil bath, maintained at 60 °C for 12 h. At the end of this period, the brown precipitate formed was collected, washed with distilled water, dried, weighed (41% yield) and kept stored in a desiccator until the moment of the analyses.

Synthesis of the $[\text{Cu}(\text{NaphPz})\text{Cl}]$ complex

To a 25-mL round bottom flask containing a solution of (E)-1-(((2-(1H-pyrazol-1-yl)ethyl)imino)methyl)naphthalen-2-ol (NaphHPz) (133 mg, 0.5 mmol) in methanol (MeOH) (2.7 mL, HPLC grade) under magnetic stirring, it was added a solution of 85 mg of $\text{CuCl}_2 \cdot 2\text{H}_2\text{O}$ in 1.1 mL of MeOH (HPLC grade), followed by further 3.5 mL of MeOH. Right after the addition of the copper salt solution, a significant color change was observed, from yellowish orange (ligand solution) to dark green. The reaction mixture was then kept under magnetic stirring at room temperature for 2 h, filtered, and the filtrate allowed to slowly concentrate over a week (kept on an undisturbed bench, at room temperature, in a vial with a needle serving as the opening on the lid). After this time, both block and needle-shaped dark green crystals were

observed on the bottom and walls of the vial, respectively. After careful decantation and drying of the solid material, 62 mg of the block-shaped crystals were isolated, corresponding to 34% yield of the desired complex.

Synthesis of the [Cu(NaphDPz)Cl] complex

To a 25-mL round bottom flask containing a solution of (E)-1-(((2-(3,5-dimethyl-1H-pyrazol-1-yl)ethyl)imino)methyl)naphthalen-2-ol (NaphHDPz) (147 mg, 0.5 mmol) in MeOH (2.7 mL, HPLC grade) under magnetic stirring, it was added a solution of 85 mg of $\text{CuCl}_2 \cdot 2\text{H}_2\text{O}$ in 1.1 mL of MeOH (HPLC grade), followed by further 3.5 mL of MeOH. Right after the addition of the copper salt solution, a significant color change was observed, from brownish (ligand solution) to deep purple. The reaction mixture was then kept under magnetic stirring at room temperature for 2 h, filtered, and the filtrate allowed to slowly concentrate over a week (kept on an undisturbed bench, at room temperature, in a vial with a needle serving as the opening on the lid). After this time, block-shaped deep purple crystals were observed and after careful decantation and drying, 60 mg of the solid material were isolated, corresponding to 31% yield of the desired complex.

Instrumental and classical analysis

^1H and ^{13}C NMR analyses were performed using CDCl_3 as the solvent on a Bruker Avance III HD-400 MHz spectrometer, operating at 400 MHz for the ^1H and 100 MHz for ^{13}C nuclei, respectively. Chemical shifts (δ) are expressed in parts per million (ppm) and were determined using the residual solvent signals as the internal references. The Attached Proton Test (APT) experiment was employed for ^{13}C NMR analysis.

FT-IR/ATR spectra of the complexes were performed using a Nicolet iS10 FT-IR spectrophotometer using an ATR accessory with Ge window.

The TGA–DSC curves were obtained using a thermal analytical system, model STA 449 F3 Jupiter® and the experimental data were obtained by Proteus® Software. For the analysis of the samples, masses near to 5.0 mg and alpha-alumina crucibles were used under air purge gas flow of 50 mL min^{-1} with heating rate optimized to $10^\circ \text{C min}^{-1}$. The copper ion in the residue of the [Cu(NaphDPz)Cl] complex was also determined by complexometric titration with a standard EDTA solution, according to the method used by Oliveira and collaborators [12].

The gaseous fragments from the thermal decomposition of the complexes were monitored using a Mettler® TGA–DSC system coupled to a Nicolet® FT-IR spectrophotometer equipped with gas cell and DTGS KBr detector. The gas cell

was kept at 250°C and the transfer line of 120 cm at 225°C . The masses of the samples for the TGA–DSC curves recording were about 10 mg with heating rate of $10^\circ \text{C min}^{-1}$ in alumina crucibles. The online FT-IR spectra were recorded with a resolution of 4 cm^{-1} .

Density functional theory (DFT) was carried out using Gaussian 16 (Revision B.01) [13] employing the HSE06 hybrid functional [14, 15] with 6-311G(d,p) basis set for C, H, N, O and Cl atoms, and LanL2DZ [16] basis set for Cu atom associated with the effective core potential (ECP). The geometry optimization was computed using Berny's optimization algorithm and the calculations of harmonic vibrational frequencies were also performed for all molecular structures. For each optimized ground state, the frequency analysis showed the absence of imaginary frequencies, confirming that the global minimum has been reached. The vertical excitation energies were calculated using time-dependent DFT (TD-DFT) methodology. Orbital molecular (MO) diagrams were reproduced using GaussView (version 6) [17]. The Polarizable Continuum Model (PCM) [18] approach was used for single point calculations in acetone.

Crystal structure

Single-crystal data were collected with a Bruker D8 Venture diffractometer operating with an Incoatec X-ray source with Montel two-dimensional optics, Ag-K α radiation ($\lambda = 0.56086 \text{ \AA}$) and a Photon 100 detector. The structures were solved by dual space methods using Bruker XT [19] and refined with Bruker XL [20] on F^2 , using anisotropic temperature parameters for all non-hydrogen atoms. The hydrogen atoms positions were calculated starting from the idealized positions. Crystal data and further details regarding the data collection and refinement for [Cu(NaphPz)Cl] and [Cu(NaphDPz)Cl] are shown in Table S1 (supplementary material). CCDC 2,018,666 and 2,018,665 contain the supplementary crystallographic data for the complexes [Cu(NaphPz)Cl] and [Cu(NaphDPz)Cl]. These data can be obtained free of charge on <http://www.ccdc.cam.ac.uk>; from the Cambridge Crystallographic Data Centre at 12 Union Road, Cambridge CB2 1EZ, UK; via fax: (+44) 1223-336-033; or via e-mail: deposit@ccdc.cam.ac.uk. Graphical representations [21] of the structures were prepared for each compound.

Results and discussion

TGA–DSC

Initially, thermogravimetric analysis (TGA) in air atmosphere was performed to establish the stoichiometry of the copper complexes. The theoretical and experimental analytical data from the TGA curves of the compounds

are in agreement with the formulas: $[\text{Cu}(\text{NaphPz})\text{Cl}]$, $[\text{Cu}(\text{NaphDPz})\text{Cl}]$ and $[\text{Cu}(\text{NaphPz})_2]$, wherein $\text{NaphPz} = (\text{E})\text{-1-}((2\text{-}(1\text{H-pyrazol-1-yl)ethyl)imino)methyl)naphthalen-2\text{-olate}$, $\text{NaphDPz} = (\text{E})\text{-1-}((2\text{-}(3,5\text{-dimethyl-1H-pyrazol-1-yl)ethyl)imino)methyl)naphthalen-2\text{-olate}$ and Cl corresponds to a chlorine atom.

The $[\text{Cu}(\text{NaphPz})\text{Cl}]$ complex, Fig. 2a, obtained in anhydrous form, is thermally stable up to 100 °C (TGA), from which temperature a small mass loss is observed, more pronounced around 200 °C with an endothermic peak at 216 °C in DSC curve. In order to assess this first mass loss step, both the peak temperature in DSC (maximum reaction) and the end of the reaction in DTG, shown in Fig. S1 (TGA–DSC/DTG) as a complement to Fig. 2a, were adopted as parameters to infer the percentage of mass loss referred to this step, which was determined at 4.0%. The correlation of these thermal events in TGA–DSC/DTG curves (supported by TGA/FT-IR section data) shows us that the mass loss in this step is due to evaporation of the solvent used in the synthesis of this compound. In addition, it was not possible to establish a defined proportion for the methanol molecule (CH_3OH) from calculation of the minimum formula and therefore, a possible coordination of methanol molecules with the metallic center can be disregarded, but is likely that part of CH_3OH exerts a strong interaction with the organic ligand, once the peak at 216 °C (DSC) shows considerable heat absorption in a small temperature range in TGA curve. Thus, the percentage of methanol is excluded, as shown in Table 1, to compose the stoichiometric ratio defined as $[\text{Cu}(\text{NaphPz})\text{Cl}]$. A solvent-free material is desirable for the compound in powder form, but the complete elimination of the solvent by heating, for instance, is difficult because whenever an operating temperature limit was established, it culminated in the start of decomposition. As a consequence, we present the results as obtained in the original synthesis, since the total elimination of all the solvent through this method was not possible. In addition, the rare microcrystals obtained in the synthesis were used for the analysis of single-crystal X-ray diffraction as a supplement to the TGA–DSC data.

Considering the second step, between 231 °C and 320 °C with mass loss of 23.52% (TGA) associated with a small exothermic peak at 278 °C in DSC curve, it can be related to the thermal decomposition of the organic ligand. This thermal event, which is not very pronounced in the DSC, shows that the decomposition products formed and consequentially released in this step react weakly with the oxidizing atmosphere used in the analysis, but with a thermal balance of released heat greater than that absorbed, i.e., ΔH less than zero. In addition, analyzing the types of bonds in the organic ligand such as C–C (346,8 kJmol^{-1}), C=C (614,2 kJmol^{-1}), C–H (413,4 kJmol^{-1}),

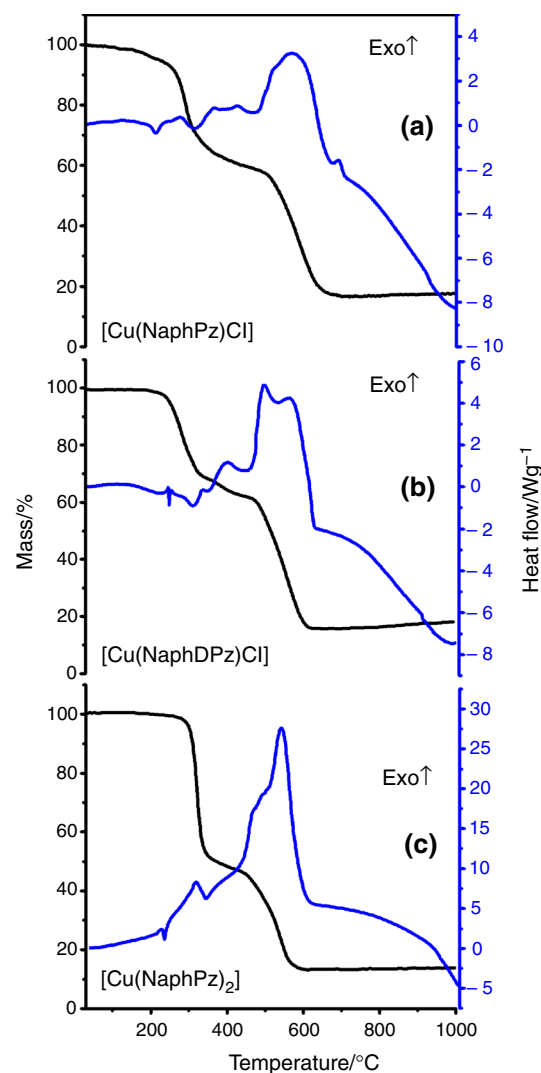


Fig. 2 (a–c) TGA–DSC curves in air atmosphere using a heating ratio of 10 °C/min and initial mass near 5.0 mg. Peaks up (exo) and peaks down (endo)

C–O (353,5 kJmol^{-1}) and C–N (305 kJmol^{-1}), C=N (600 kJmol^{-1}), N–N (163 kJmol^{-1}), N=N (409 kJmol^{-1}) it is possible to theoretically insert, based on the binding energies and typical interatomic distances [22, 23], that the fragmentation of the organic ligand must begin through lower energy chemical bonds. The third step, with a slow mass loss of 13.48%, between 320 and 475 °C (TGA), produces two small exothermic peaks at 368 and 427 °C probably related to the fragmentation of the open chain (-C-C-N=C-) and formation of remaining stable material from the cyclical part of the ligand. Finally, the last step, with mass loss of 40.30% between 475 and 690 °C (TGA) associated with an intense exothermic peak at 571 °C (DSC), occurs due to oxidation/combustion of the organic matter, as well as fragmentation of Cu–Cl bond

Table 1 Analytical and thermoanalytical (TGA) data of the compounds; in which Cu = copper; NaphPz and NaphDPz = ligands

| Compounds | Ligand/% | | Residue (CuO)/% | | Methanol* /% | |
|----------------------------|----------|-------|-----------------|-------|--------------|------|
| | Calc | TGA | Calc | TGA | Calc | TGA |
| [Cu(NaphPz)Cl] | 78.10 | 78.30 | 21.90 | 21.70 | – | 4.0* |
| [Cu(NaphDPz)Cl] | 79.67 | 79.05 | 20.33 | 2.95 | – | 2.8* |
| [Cu(NaphPz) ₂] | 86.57 | 86.28 | 13.43 | 13.72 | – | – |

Calc. = calculated, Excluding the methanol solvent (%) for the stoichiometric calculus

[24], leading to formation of an apparently stable residue, but which slowly gains mass (1.00%) up to around 950 °C. This small mass gain is probably due to oxidation of metallic copper in the Cu and CuO mixture, data which at 950 °C (TGA) were used to calculate the stoichiometry.

For [Cu(NaphDPz)Cl] complex, Fig. 2b, the synthesis was performed in the same experimental conditions as those of [Cu(NaphPz)Cl]. In the TGA–DSC curves, between 192 and 250 °C, it is possible to highlight a small constant mass loss that becomes more accentuated after 242 °C, with an endothermic peak at 249 °C. To determine the final temperature of the reaction, the peak temperature in the DTA (maximum reaction ratio) and final temperature onset were adopted. However, for this compound, as the first mass loss is constant, the TGA curve does not present a maximum inflection point and as a consequence, no defined peak in the DTG curve. Thus, similarly to what was previously described for [Cu(NaphPz)Cl], this mass loss is also due to evaporation of the solvent methanol used in the synthesis of this complex, so that it is possible to assume that part of the methanol solvent molecules also exerts a strong interaction with the organic ligand. The inferred data for the first mass loss step (2.8%) of [Cu(NaphDPz)Cl] compound can be better supported by Fig. S2 (TGA–DSC/DTG), of the supplementary material.

For the second step, considering the mass loss interval between 250 and 360 °C, with mass loss of 30.2% in TGA curve, it is necessary to carefully evaluate the DSC curve after the end of first step because an exothermic event occurs superimposed immediately after the endothermic peak in the first stage at 249 °C, giving the impression that an endothermic peak at 310 °C is present. Therefore, it is correct to affirm that the valley at 310 °C is due to the return of the baseline to the beginning of a new exothermic event with a peak temperature at 335 °C. Furthermore, the fragments released in this step are more stable, reacting less intensely with the oxidized atmosphere. In the third step, between 370 °C and 470 °C (TGA), a relatively small mass loss of 5.64% is observed, which is signaled by an exothermic peak in the DSC curve at 370 °C. Thus, based on the binding energies it is possible that this mass loss is due to thermal decomposition of part of the acyclic chain (–C–C–N=C–), besides fragments of dimethylpyrazole. The last mass loss of 45.6%, precisely between 470 and 620 °C (TGA), is related

to the oxidation/combustion of the cyclical and/or aromatic part of the ligand and rupture of the Cu–Cl bond, leading to formation of an apparently stable residue, but which slowly gains mass (2.39%) up to around 950 °C. As a result, other TGA–DSC analyses were carried out, which reproduced the same result, thus discarding possible problems or equipment calibration errors. The residue was then evaluated visually and using classical techniques at two different temperatures, at 650 °C and at the final temperature of analysis (950 °C). The visual evaluations showed a completely black residue at both temperatures, which excludes the formation of a mixture of oxides or copper (I) oxide. A qualitative test at 650 °C for chloride showed no evidence of this ion in the residue and finally, complexometric analysis showed a copper content of 99.3%. Therefore, from these results, we concluded that this small mass gain is due to the oxidation of metallic copper particles, probably produced from copper reduction by the carbonaceous material (reducing agent) and/or by the chloride ions [25].

The last synthesized complex [Cu(NaphPz)₂], Fig. 2c, was obtained in the absence of chloride and through the reaction of copper carbonate with the ligand in its acid form. This compound is stable up to 215 °C and presents a thermal behavior slightly different from the other two compounds studied. The melting peak temperature in DSC curve, in air atmosphere, is shown at 227 °C.

For [Cu(NaphPz)₂] complex, the first thermal decomposition step in air atmosphere starts at around 260 °C and ends at 326 °C, with a mass loss of 40.85% (TGA) associated with a small exothermic peak in the DSC curve at 310 °C. This marked mass loss step, which coincides with pyrazole fragments and the open chain (40.85%) of the two ligands coordinated to the metal center, shows that the fragmentation way is highly dependent on chemical environment. Thus, it is possible that the second mass loss step is inherent to the thermal decomposition of the more stable fraction of the ligand, part of the cyclic/aromatic portion. In this step, the 12.00% mass loss (TGA), between 326 and 435 °C is signaled in DSC curve by an exothermic event (shoulder) starting at 336 °C. The last step, between 435 and 607 °C, with mass loss of 33.43% (TGA) associated with an intense exothermic peak at 535 °C is due to oxidation/combustion of the organic matter, leading to formation of copper oxide (CuO) as final residue.

Complementing the thermal analysis study, the gaseous products released in each step of the TGA-DTA curves were monitored on-line and identified by TGA/FT-IR system; such study will be better discussed further.

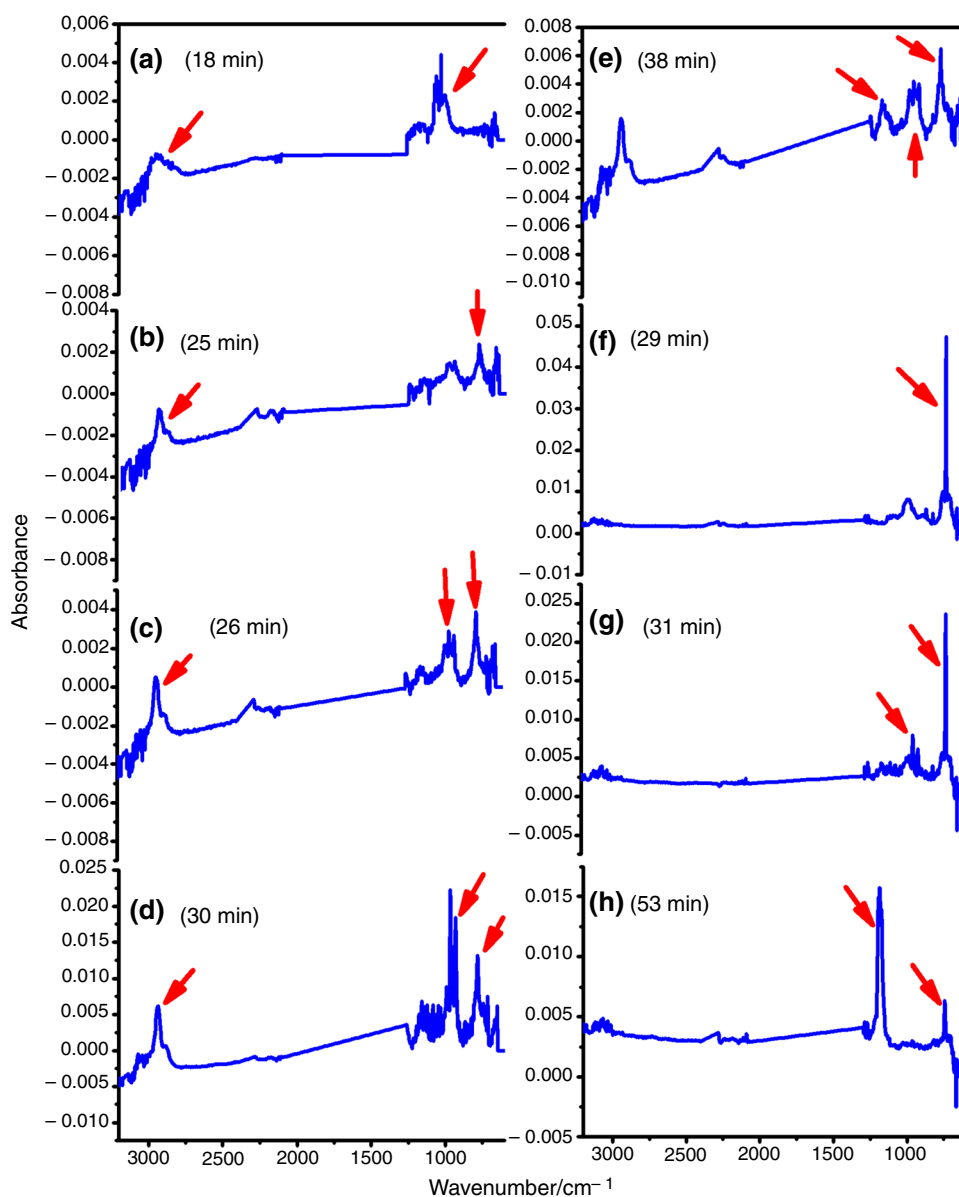
Evolved gas analysis

In addition to the results obtained by TGA-DSC on stoichiometry and thermal behavior of the compounds, the gaseous products were also monitored step by step through a TGA-DSC/FT-IR system under air and nitrogen atmospheres, and the same products were detected under both atmospheres. However, in air atmospheres the release of gaseous products like carbon dioxide (CO₂) and carbon monoxide (CO), produced from the organic matter decomposition,

overlap the release of most of the organic fragments. Thus, the gaseous products evolved for copper complexes from the thermal decomposition were monitored in inert atmosphere (N₂), and the corresponding data is shown in Fig. 3a–h. The FT-IR spectra obtained on-line were evaluated based on data available in the literature [26, 27] and by digital spectral library-based, provided by OMNIC®.

The first gaseous product released and identified from the thermal decomposition of [Cu(NaphPz)Cl] and [Cu(NaphDPz)Cl] complexes was only methanol, according to Fig. 3a. The FT-IR spectra obtained around 15 min or at 180 °C (TGA) corroborate the data discussed in the section of TGA-DSC analysis, wherein the first endothermic event in each DSC curve is due to evaporation of the methanol solvent used in the synthesis of the compounds. The gaseous

Fig. 3 Representative FT-IR spectra for the main gaseous products monitored, in nitrogen atmosphere, during the thermal decomposition of the complexes



methanol (CH₃OH) produces a set of characteristic peaks at 1008, 1033 and 1062 cm⁻¹, in addition to a band between 3000 and 2800 cm⁻¹ related to C–H stretches.

For the [Cu(NaphDPz)Cl] complex, above 245 °C (TGA), one peak highlighted at 783 cm⁻¹ (FT-IR), related to fragments of dimethylpyrazole, can be observed in Fig. 3b; subsequently, at 248 °C, it is also possible to observe peaks at 992, 965 and 930 cm⁻¹ related to ammonia, according Fig. 3c. Regarding the fragments released in form of ammonia, Fig. 3d, these are more pronounced around 300 °C (TGA) and then decreases up to 450 °C. At the same time, when there is a decrease in gaseous products, new bands in the region 1100–1200 cm⁻¹, above 450 °C, are now also observed in Fig. 3e. These bands are probably related to fragments (–C–C–)_n of the aromatic part of the ligand, which is more stable and decomposes at higher temperature.

For [Cu(NaphPz)₂] complex, the first fragment observed at 245 °C is pyrazole at 744 cm⁻¹ (Fig. 3f), as well as for [Cu(NaphPz)Cl] complex around 260 °C, after elimination of methanol solvent, as previously discussed. In these compounds, similarly to [Cu(NaphDPz)Cl] complex, it is observed the release of ammonia shortly after pyrazole fragment, as shown in Fig. 3g, so that these two fragments are observed in the FT-IR spectra up to close to 500 °C, that is, for [Cu(NaphPz)₂] and [Cu(NaphPz)Cl] complexes. Above this temperature, Fig. 3h, ammonia-free fragments are observed, with emphasis on pyrazole fragment that continues to be released in a lower proportion, which is probably accompanied by fragments such as (–C–C–N–C–)_n or even for fragments involving C–O bond due to an intense peak at 1182 cm⁻¹. According to the literature, this peak can be characteristic of secondary aliphatic amines [26, 27], while for C–O bond, the probable possibility is the fragmentation of the aromatic part to produce gaseous products like (–C–O–C–)_n, which is plausible for high temperatures.

In summary, taking the majority of fragments monitored through TGA/FT-IR and the theoretical binding energies that involve the organic ligand into account, it is possible to make some kind of logical association of the approximate

pattern that the thermal degradation follows. Thus, in this process the appearance of pyrazole or methylpyrazole, followed by the gaseous product ammonia is observed at first, which shows that fragmentation begins with lower energy bonds such as N–N and C–N. As the temperature increases, peaks can be seen in the FT-IR fingerprint region, which may be related to fragments from the breaking of C–C and/or C–O bonds. Furthermore, although the degradation does not occur in a homogeneous and sequential manner, it is possible that the formation of products arising from the breaking of stronger bonds C=C or C=N of the aromatic part will occur last, due to the stability that the ring provides to the system.

Crystalline structure

The complexes were previously characterized by thermogravimetry and simultaneous differential scanning calorimetry (TGA–DSC) to determine the stoichiometric ratio, while the structural arrangement for [Cu(NaphPz)Cl] and [Cu(NaphDPz)Cl] complexes was determined using single-crystal X-ray diffraction. The structure for [(Cu(NaphPz)₂] complex has not been determined due to the absence of suitable single-crystals for this material.

The molecular structures for the mononuclear [Cu(NaphPz)Cl] and [Cu(NaphDPz)Cl] complexes, designed with DIAMOND [20], are shown in Fig. 4.

In each complex, the Cu^{II} atom is chelated by a (N,N,O)-tridentate Schiff-base and a chloride ligand. For complex [Cu(NaphPz)Cl], the Cu^{II} atom adopts a distorted square planar environment, in agreement with the T parameter. The geometry can be confirmed from the geometric parameter τ by applying the following calculation: $T_4 = 360^\circ - (\alpha - \beta) / 141^\circ$, for structures with coordination number four. The values of T_4 will range from 1.00—for a perfect tetrahedral geometry—to zero—for a perfect square planar geometry. Intermediate structures, including trigonal pyramidal and seesaw, are in the range of 0 to 1.00 [28]. For the [Cu(NaphPz)Cl] complex, $T_4 = 0.07$, and as the value is

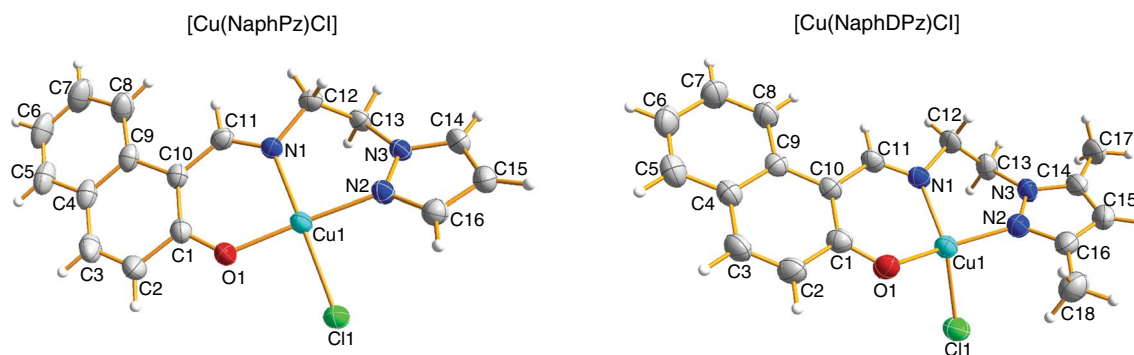


Fig. 4 Molecular structure of the [Cu(NaphPz)Cl] and [Cu(NaphDPz)Cl] complexes. The thermal ellipsoids indicate the 50% probability level

close to zero, it confirms the distorted square-planar geometry; for the [Cu(NaphDPz)Cl] complex, $T_4=0.41$, confirming the seesaw geometry, respectively, as shown in Fig. 5. It has been seen that other copper complexes show seesaw coordination geometry [27]. The angles α and β used for the calculations are described in Table S2 of the supplementary material. The difference in the coordination geometry of [Cu(NaphPz)Cl] and [Cu(NaphDPz)Cl] is due to the spatial orientation of the methyl groups in the ligand of the latter complex.

For the (N,N,O)-tridentate Schiff-base and chloride ligand, the bond lengths to the metal center in [Cu(NaphPz)Cl] complex are Cu(1)–O(1) (1.9051(15) Å, Cu(1)–N(1) (1.9756(16) Å, Cu(1)–N(2) (2.0026(17) Å and Cu(1)–Cl(1) (2.2765(6) Å. For [Cu(NaphDPz)Cl] complex, these bond lengths are Cu(1)–O(1) 1.876(2) Å, Cu(1)–N(1) 1.950(3) Å, Cu(1)–N(2) 1.972(3) Å and Cu(1)–Cl(1) 2.2783(11). Both sets of bond lengths are in agreement with those reported for other copper(II) complexes containing (N,N,O)-tridentate Schiff-base and chloride ligand [10, 29].

The angles (in degrees) for the bonding in [Cu(NaphPz)Cl] complex are O(1)–Cu(1)–N(1) (90.84(7), O(1)–Cu(1)–N(2) (175.62(7), N(1)–Cu(1)–N(2) (92.27(7), O(1)–Cu(1)–Cl(1) (88.15(5), N(1)–Cu(1)–Cl(1) (173.85(5) and N(2)–Cu(1)–Cl(1) (89.07(5); for [Cu(NaphDPz)Cl] complex, the bonding angles are O(1)–Cu(1)–N(1) 93.18(11), O(1)–Cu(1)–N(2) 154.38(12), N(1)–Cu(1)–N(2) 93.29(12), O(1)–Cu(1)–Cl(1) 92.07(8), N(1)–Cu(1)–Cl(1) 148.34(9) and N(2)–Cu(1)–Cl(1) 95.31(9). The changes observed, from one complex to the other, confirm the distortion in the coordination geometry caused by the spatial orientation of the methyl group.

Infrared spectroscopy: theoretical and experimental

On the basis on experimental TGA–DSC and FT-IR data obtained from the complexes, a theoretical calculation employing quantum chemical approach was performed to obtain theoretical FT-IR spectra, in addition to the experimental data, as shown in Fig. 6, wherein (a*–c*) represents

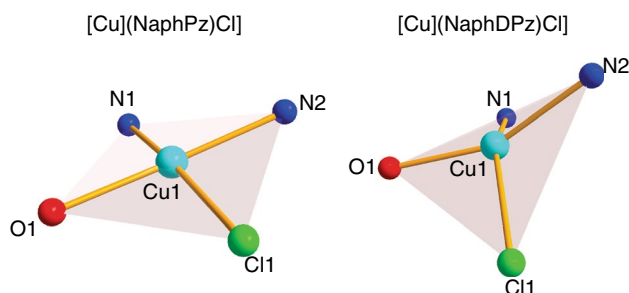


Fig. 5 Coordination polyhedron of Cu^{II} center in [Cu(NaphPz)Cl] and [Cu(NaphDPz)Cl] complexes

the theoretical* data and (a–c) the experimental ones. The optimization of the molecular geometry structures of the compounds studied was performed using Berny's optimization algorithm, and the calculations of harmonic vibrational frequencies were also performed for all molecular structures. However, in the correlation between theoretical and experimental spectra, it is observed small differences in shape and number of bands, given that theoretical calculation is performed on the basis of a single molecule without taking the interference of molecular interaction into account for calculating FT-IR. However, the main bands can be observed in the spectra without any prejudice to the interpretation.

For [Cu(NaphPz)Cl] and [Cu(NaphDPz)Cl] complexes between 3500 and 2900 cm⁻¹ (Fig. S3), a band was observed with the maximum at around 3400 cm⁻¹ and relatively high peaks around 3000 cm⁻¹, when this region is compared to that one of the [Cu(NaphPz)] compound, which presents in the same region only stretches related to the C-H bond. This observation corroborates the experimental data determined by TGA–DSC and TGA/FT-IR, related to the release of the methanol solvent, used in the synthesis of the two complexes.

In relation to the spectra fingerprint region, the theoretical* and experimental data, Fig. 6 (a*–c* and a–c) lead to a convergent correlation, with displacements around 20 cm⁻¹ for the main bands. In this sense, the following correlations can be made, so that in the 1600 cm⁻¹ region there is an overlap of bands attributed to C=C and C=N stretching, as well as in 1400–1000 cm⁻¹ region, assigned to the bending in the plane mode. Around 800 cm⁻¹ it is observed the out-of plane bending for OCC bonds, while the bands near 750 cm⁻¹ can be assigned to torsional mode for HCCC and HCCN bonds. Therefore, from these correlations it is possible to suggest that the optimized structures through theoretical calculation are in line with the experimental results presented.

UV–Vis absorption study

The [Cu(NaphPz)Cl], [Cu(NaphDPz)Cl] and [Cu(NaphPz)₂] complexes, solubilized in acetone, were analyzed by UV–Vis spectrometry and the experimental results obtained compared to the DFT calculation, as shown in Fig. 7. Although the acetone solvent has maximum absorption at 210 and 280 nm, close to the wavelengths under study (327 nm and 450 nm), there was no interference of the solvent in the absorption of the complexes, using them at a concentration of 1.0 × 10⁻⁵ molL⁻¹. Optimized molecular structures of the complexes were evaluated using time-dependent DFT (TD-DFT) methodology to show the spatial distribution of charges in highest occupied molecular orbitals (HOMO) and lowest unoccupied molecular orbitals (LUMO), in order to indicate how the electron transport in the systems occurs.

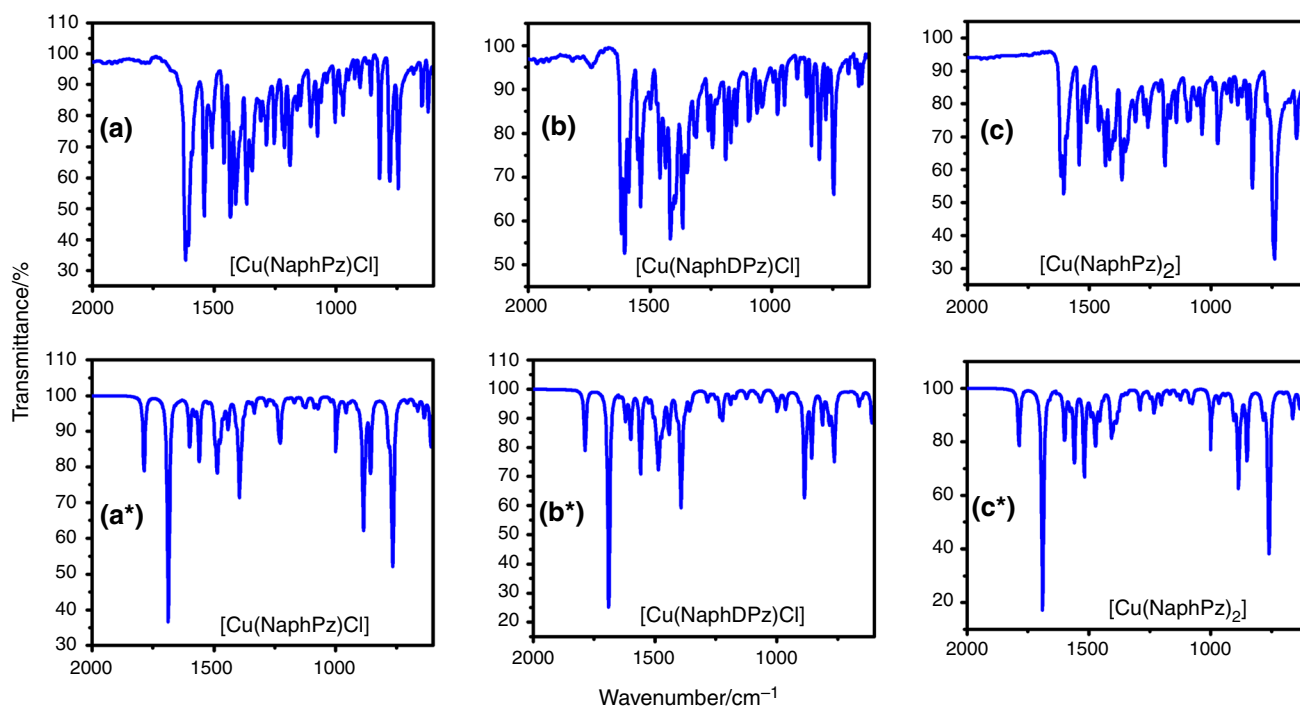


Fig. 6 FT-IR Spectra (2000–600 cm^{-1}): experimental (a, b and c) and theoretical (a*, b* and c*) for the synthesized complexes

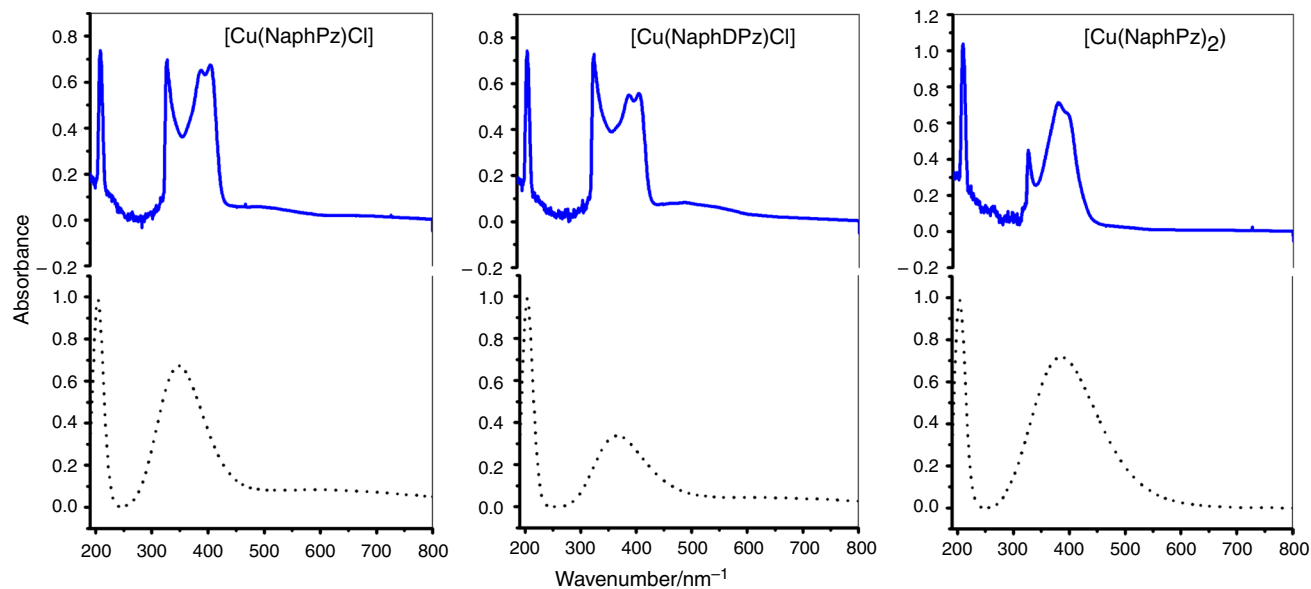


Fig. 7 Experimental (—) and theoretical (····) UV-Vis spectra for [Cu(NaphPz)Cl], [Cu(NaphDPz)Cl] and [Cu(NaphPz)₂] complexes

To define how the electrons are distributed among the orbitals of the complexes, we use as a base the ligand donor–acceptor character, defined by the spectrochemical series, as well as single-crystal geometry obtained by X-ray diffraction data for [Cu(NaphPz)Cl] and [Cu(NaphDPz)Cl] complexes. In these mononuclear Cu(II) complexes, the metal atom is chelated by a tridentate (N,N,O)-Schiff

base and a chloride ligand; therefore, it is possible to define that the [Cu(NaphPz)₂] complex, obtained in powder form with two Schiff base units, has a coordination number equal to 6. In addition, the copper (II) ion with d^9 configuration, regardless of the ligand, suffers geometry distortion defined as Jahn–Teller effect [30], which compresses the structure in the z-axis direction followed by a decrease in band gap

energy between HOMO/LUMO orbitals. From the main characteristics of the metal–ligand binding presented, we can then state that the charge distribution in these complexes is carried out through bindings with π character orbitals ($p\pi-d\pi$), which are favored by the chloride ligand and the Schiff base oxygen atom. Another bonding character that can be identified is that of ($d\pi-p\pi^*$) type, which are electron donations from the filled d orbitals to the π^* orbitals, involving Schiff base nitrogen atoms.

From the charge distributions, obtained by DFT calculations, for the frontier molecular orbitals (FMO) HOMO \rightarrow LUMO of major contributions, according Fig. S4, in the [Cu(NaphPz)Cl] and [Cu(NaphDPz)Cl] complexes with similar structures, the charge distribution between them is slightly differentiated, probably due to methyl groups. This information can be better corroborated remembering that [Cu(NaphDPz)Cl] presents a very distorted tetrahedral geometry described as a seesaw, as shown in Fig. 4. Concomitantly, the description of charge transfer (CT) on the complexes studied, as shown in Fig. S4, can be summarized by metal (M), Schiff base (L) and halide (X) interactions, as well as that of intraligand transfer (IL). Thus, for the [Cu(NaphPz)Cl] complex, the HOMO/LUMO orbitals with major contribution, Fig. S4, and oscillator strength (f) are shown as follow: H-1 β \rightarrow L β (69%, $f=0.0021$), H β \rightarrow L β (46%, $f=0.0000$), H α \rightarrow L + 1 α (47%, $f=0.0000$) and H-3 β \rightarrow L β (43%, $f=0.0255$); for the [Cu(NaphDPz)Cl] complex H α \rightarrow L α (44%, $f=0.0004$), H β \rightarrow L + 1 β (46%, $f=0.0004$), H-4 β \rightarrow L β (45%, $f=0.0003$) and H-5 β \rightarrow L β (37%, $f=0.0564$) and, for Cu(NaphPz)₂ complex, H α \rightarrow L + 1 α .

(24%, $f=0.0003$), H-1 β \rightarrow L + 1 β (27%, $f=0.0003$), H-1 β \rightarrow L β (88%, $f=0.0040$) and H β \rightarrow L β (36%, $f=0.0040$).

For a general approach, evaluating the CT by HOMO \rightarrow LUMO orbitals for the complexes, a larger charge displacement is observed on the naphthalene conjugate system for [Cu(NaphDPz)Cl] complex than for the [Cu(NaphPz)Cl] complex, since there is a charge transfer from metal and halide orbitals mixture (M + X) to Schiff's base ligand (L). This effect, clearly seems to be caused by the addition of two alkyl groups to the pyrazole aromatic ring that acts as an electron "pusher" for the system. On the other hand, for the hexa-coordinated [Cu(NaphPz)₂] complex, it is observed that the absence of the chloride ligand favors a preferential charge distribution, probably directed by the nitrogen atoms that are part of the naphthalene ring conjugate system, as well as by the Schiff's base oxygen atoms linked to the metal center. In this case, the nitrogen atoms in the pyrazole aromatic ring act as electron donors, as it can be verified by the charge distribution along the LUMO orbitals.

Conclusions

Copper (II) mononuclear complexes in anhydrous form, using an unprecedented Schiff-base ligand were synthesized and characterized in the solid state or solution by thermoanalytical methods (TGA–DSC, TGA/FT-IR), single crystal X-ray diffraction, FT-IR, UV–Vis and DFT calculations.

Based on the TGA–DSC thermoanalytical data, it was possible to define the stoichiometric ratio of the synthesized complexes, thermal stability, decomposition temperatures, as well as the temperature of formation of the final residue used in the calculation of stoichiometry. The online monitoring of the main volatile products related to thermal decomposition, performed by TGA/FT-IR, shows that the complexes obtained in methanol solvent medium adsorbed a small amount of the solvent, while the complex obtained in ethanol/water was solvent free.

From single-crystal X-ray diffraction data, it was possible to establish that the chloride and Schiff-base ligands are coordinated to the central ion with coordination number four, forming structures of distorted square-planar geometry for [Cu(NaphPz)Cl] complex and seesaw geometry for [Cu(NaphDPz)Cl] complex. The geometry could be confirmed from the geometric parameter τ_4 . For [Cu(NaphPz)] obtained in powder form with stoichiometry defined by TGA–DSC, it is possible to state that it is a hexa-coordinated complex.

Regarding UV-Vis and FT-IR experimental data, they were supported by DFT calculations and showed high correlation for the optimized geometries, from which it was possible to demonstrate how HOMO \rightarrow LUMO charge transfer occurs in the studied systems.

Supplementary Information The online version contains supplementary material available at <https://doi.org/10.1007/s10973-021-10803-5>.

Acknowledgements The authors thank Brazilian Foundations CNPq, Fundect, Capes and Finep for financial support, and are grateful to Professor Massao Ionashiro for allowing us to carry out measurements in the Ivo Giolito Thermal Analysis Laboratory (LATIG) – UNESP, and Professional Noemi Marques de Carvalho for English reviewing.

References

1. Ansari A, Ali A, Asif M, Shamsuzzaman. Review: biologically active pyrazole derivatives. *New J Chem.* 2017;41:16–41.
2. Faria JV, Vegi PF, Miguita AGC, Santos MS, Boechat N, Bernardino AMR. Recently reported biological activities of pyrazole compounds. *Bioorg Med Chem.* 2017;25:5891–903. <https://doi.org/10.1016/j.bmc.2017.09.035>.
3. Khan MF, Alam MM, Akhtar GVW, Akhter M, Shaquiquzzaman M. The therapeutic voyage of pyrazole and its analogs: a review. *Eur J Med Chem.* 2016;120:170–201. <https://doi.org/10.1016/j.ejmech.2016.04.077>.

4. Fustero S, Sánchez-Roselló M, Barrio P, Simón-Fuentes A. From 2000 to mid-2010: a fruitful decade for the synthesis of pyrazoles. *Chem Rev.* 2011;111:6984–7034.
5. Gupta KC, Sutar AK. Catalytic activities of Schiff base transition metal complexes. *Coord Chem Rev.* 2008;252:1420–50.
6. Abu-Dief AM, Mohamed IMA. A review on versatile applications of transition metal complexes incorporating Schiff bases. *Beni-Seuf Univ J Appl Sci.* 2015;4:119–33.
7. Silva F, Marques F, Santos IC, Paulo A, Rodrigues AS, Rueff J, Santos I. Synthesis, characterization and cytotoxic activity of gallium(III) complexes anchored by tridentate pyrazole-based ligands. *J Inorg Biochem.* 2010;104:523–32. <https://doi.org/10.1016/j.jinorgbio.2010.01.003>.
8. Ainooson MK, Guzei IA, Spencer LC, Darkwa J. Pyrazolylimine iron and cobalt, and pyrazolylimine nickel complexes: synthesis and evaluation of nickel complexes as ethylene oligomerization catalysts. *Polyhedron.* 2013;53:295–303.
9. Yankey M, Obuah C, Darkwa J. Phenoxysalicylaldimine-bearing Chromium(III) precatalysts for ethylene polymerization. *Macromol Chem Phys.* 2014;215:1767–75.
10. Gama S, Mendes F, Marques F, Santos ICM, Carvalho MF, Correia I, Pessoa JC, Santos I, Paulo A. Copper(II) complexes with tridentate pyrazole-based ligands: synthesis, characterization, DNA cleavage activity and cytotoxicity. *J Inorg Biochem.* 2011;105:637–44. <https://doi.org/10.1016/j.jinorgbio.2011.01.013>.
11. Hamann JN, Tuczec F. New catalytic model systems of tyrosinase: fine tuning of the reactivity with pyrazole-based N-donor ligands. *Chem Commun.* 2014;50:2298–300.
12. Oliveira CN, Ionashiro M, Graner CAF. Titulação complexométrica de zinco, cobre e cobalto. *Ecl Quim J.* 1985;10:7–10.
13. Frisch MJ, Trucks GW, Schlegel HB, Scuseria GE, Robb MA, Cheeseman JR, Scalmani G, Barone V, Petersson GA, Nakatsuji H, Li X, Caricato M, Marenich AV, Bloino J, Janesko BG, Gomperts R, Mennucci B, Hratchian HP, Ortiz JV, Izmaylov AF, Sonnenberg JL, Williams-Young D, Ding F, Lipparini F, Egidi F, Goings J, Peng B, Petrone A, Henderson T, Ranasinghe D, Zakrzewski VG, Gao J, Rega N, Zheng G, Liang W, Hada M, Ehara M, Toyota K, Fukuda R, Hasegawa J, Ishida M, Nakajima T, Honda Y, Kitao O, Nakai H, Vreven T, Throssell K, JrJA Montgomery, Peralta JE, Ogliaro F, Bearpark MJ, Heyd JJ, Brothers EN, Kudin KN, Staroverov VN, Keith TA, Kobayashi R, Normand J, Raghavachari K, Rendell AP, Burant JC, Iyengar SS, Tomasi J, Cossi M, Millam JM, Klene M, Adamo C, Cammi R, Ochterski JW, Martin RL, Morokuma K, Farkas O, Foresman JB, Fox DJ. *Gaussian 16 (B.01)*. Wallingford, CT: Gaussian Inc.; 2016.
14. Heyd J, Scuseria G. Efficient hybrid density functional calculations in solids: the HS-Ernzerhof screened Coulomb hybrid functional. *J Chem Phys.* 2004;121:1187.
15. Heyd J, Scuseria GE. Assessment and validation of a screened Coulomb hybrid density functional. *J Chem Phys.* 2004;120:7274. <https://doi.org/10.1063/1.1668634>.
16. Hay PJ, Wadt WR. Ab initio effective core potentials for molecular calculations - potentials for K to Au including the outermost core orbitals. *J Chem Phys.* 1985;82:299.
17. Dennington R, Keith TA, Millam JM. *GaussView (version 6)*. Shawnee Mission: Semichem Inc; 2019.
18. Miertuš S, Scrocco E, Tomasi J. Electrostatic interaction of a solute with a continuum. A direct utilization of ab initio molecular potentials for the prevision of solvent effects. *Chem Phys.* 1981;55:117.
19. Sheldrick GM. SHELXT – Integrated space-group and crystal-structure determination. *Acta Crystallogr Sect A Found Crystallogr.* 2015;71:3–8.
20. Sheldrick GM. Crystal structure refinement with SHELXL. *Acta Crystallogr Sect C Struct Chem.* 2015;C71:3–8.
21. Brandenburg K, Putz H. *DIAMOND – a program for the representation of crystal structures version 463*, Crystal Impact, Bonn, Germany. 2020. <https://www.crystalimpact.com/diamond/references.htm>.
22. Orpen AG, Brammer L, Allen FH, Kennard O, Watson DG, Taylor R. Appendix A: typical interatomic distances in organic compounds and organometallic compounds and coordination complexes of the d- and f-block metals. New Jersey: Wiley; 1994.
23. Luo YR. *Comprehensive handbook of chemical bond energies*. 1st ed. FL: CRC Press; 2007.
24. Yesilkaynak T, Emen FM, Avsar G, Kulcu N. The preparation and characterization of dichlorobispyridinecopper(II) complex and its intermediates. *J Therm Anal Calorim.* 2015;122:1493–502. <https://doi.org/10.1007/s10973-015-4749-z>.
25. Liu D, Chen Xin, Bian B, Lai Z, Situ Y. Dual-Function Conductive Copper Hollow Fibers for Microfiltration and Anti-biofouling in Electrochemical Membrane Bioreactors. *Front Chem.* 2018. <https://doi.org/10.3389/fchem.2018.00445>.
26. Nakamoto K. *Infrared and raman spectra of inorganic and coordination compounds: part a: theory and applications in inorganic chemistry*. 6th ed. Hoboken: Wiley; 2008.
27. Pavia DL, Lampman GM, Kriz GS, Vyvyan JA. *Introduction to Spectroscopy*. 4th ed. Toronto: Nelson Education; 2008.
28. Yang L, Powell DR, Houser RP. Structural variation in copper(I) complexes with pyridylmethylamide ligands: structural analysis with a new four-coordinate geometry index τ_4 . *Dalton Trans.* 2007. <https://doi.org/10.1039/B617136B>.
29. Ma Shu-Lan, Sun Xu-Xia, Song G, Qi Chuan-Min, Huang Hai-Bo, Zhu Wen-Xiang. A new chloro-bridged cu(II) schiff base complex with ferromagnetic exchange interaction. *Eur J Inorg Chem.* 2007. <https://doi.org/10.1002/ejic.200600890>.
30. Widerski GS, Wiśłocka RS, Łyszczek R, Wojtulewski S, Samsonowicz M, Lewandowski W. Thermal, spectroscopic, X-ray and theoretical studies of metal complexes (sodium, manganese, copper, nickel, cobalt and zinc) with pyrimidine-5-carboxylic and pyrimidine-2-carboxylic acids. *J Therm Anal Calorim.* 2019;138:2813–37. <https://doi.org/10.1007/s10973-019-08594-x>.

Publisher's Note Springer Nature remains neutral with regard to jurisdictional claims in published maps and institutional affiliations.